FULL PAPER

Contact Electrification

ADVANCED
FUNCTIONAL
MATERIALS

www.afm-journal.de

Effects of Metal Work Function and Contact Potential Difference on Electron Thermionic Emission in Contact Electrification

Cheng Xu, Binbin Zhang, Aurelia Chi Wang, Wenzhe Cai, Yunlong Zi, Peizhong Feng, and Zhong Lin Wang*

Triboelectric nanogenerator (TENG) is a direct measure of the surface charge density, thus providing a novel and powerful tool to study the essential mechanism of contact electrification (CE). A variety of TENGs including a Pt-Al$_2$O$_3$ TENG, Au-Al$_2$O$_3$ TENG, Ti-Al$_2$O$_3$ TENG, Al-Al$_2$O$_3$ TENG, and SiO$_2$-Al$_2$O$_3$ TENG are prepared in this study. After introducing initial charges on the Al$_2$O$_3$ surface of the TENGs, the long-term evolution of surface charge quantity is investigated at different temperatures. The results show that charge variation of all the TENGs is analogous to exponential decay and is in accord with the thermionic emission model, verifying the electron transfer dominated mechanism of CE. Additionally, it is explored for the first time that the potential barrier of materials can be regulated by changing the contacting metals or dielectrics. Regulation of the barrier at high temperatures fully excludes the influence of ions from moisture and functional groups, which further indicates the dominant role played by electron transfer in CE. Surface state models for explaining barrier regulation during CE for both metal–dielectric and dielectric–dielectric pairs are proposed. This study provides a new perspective of the exploration of CE, and a novel method for further increasing or rapidly eliminating electrification of charged materials.

1. Introduction

The contact and separation of two materials generates contact electrification (CE) (or triboelectrification), and the triboelectric nanogenerator (TENG) was invented accordingly.[1,2] The TENG has opened up a special field of energy transfer via the efficient collection of mechanical energy and has been widely used in a variety of areas including environmental sensing, wearable electronic devices, human–machine interfacing, as well as blue energy.[3–10] The rapid development of the TENG led to a reconsideration of the core mechanisms of CE, such as the characteristics of transferred charges and the reason for long-term maintenance of generated charges on the surface of materials.[11,12] Since CE was first recorded 2600 years ago in ancient Greek, its mechanism remains one of the oldest unsolved problems in the world.

It is well known that CE generates charge transfer. During a long period, there has been an argument on what the charge identity is—electrons or ions.[13,14] The electron transfer model has claimed that CE occurs from electron transfer between contacting materials.[15,16] The complicated ion transfer model put forward the necessity of ions as carriers in charge transfer.[17,18] It suggests that there are both positive and negative ions on the surface of materials, with one being fixed on the surface and another able to move freely in order to bring about electrification.[19] To account for the lack of mobile ions on the surfaces of nonionic polymers, it was further speculated that ambient moisture could form hydroxide and hydrogen ions, which would lead to ion transfer and then generate CE.[20] Our previous study managed to exclude the effect of ions formed from ambient moisture via charge transfer temperatures above the boiling point of water, and we found that charge evolution was consistent with the

Dr. C. Xu, Prof. Z. L. Wang
Beijing Institute of Nanoenergy and Nanosystems
Chinese Academy of Sciences
Beijing 100083, China
E-mail: zhong.wang@mse.gatech.edu

Dr. C. Xu, B. Zhang, A. C. Wang, Dr. Y. Zi, Prof. Z. L. Wang
School of Materials Science and Engineering
Georgia Institute of Technology
Atlanta, GA 30332-0245, USA

Dr. C. Xu, W. Cai, Prof. P. Feng
School of Materials Science and Engineering
China University of Mining and Technology
Xuzhou 221116, China

Dr. Y. Zi
Department of Mechanical and Automation Engineering
The Chinese University of Hong Kong
Shatin, N.T., Hong Kong SAR, China

Prof. Z. L. Wang
School of Nanoscience and Technology
University of Chinese Academy of Sciences
Beijing 100049, China

exponential decay through the electron thermionic emission equation, which confirmed the electron transfer dominated mechanism of CE.[21,22] In addition, it first revealed that the potential barrier on materials' surfaces was the key for preventing charges from escaping. However, the specific features of the potential barrier and its influencing factors are unclear. Moreover, further studies are still needed to improve the verification and understanding of the dominating mechanism of electron transfer in CE.

In the present study, a variety of high-temperature-resistant TENGs were designed and prepared, including metal–dielectric TENGs and dielectric–dielectric TENGs. Long-term evolution of initial charges introduced to material surfaces was investigated at different high temperatures. It showed that charge evolution at high temperatures of both metal–dielectric TENGs and dielectric–dielectric TENGs was in accord with the exponential decay of thermionic emission, verifying that electron transfer was the dominating mechanism of CE between two solids. Additionally, it was found that the potential barrier on a material surface could alter slightly according to different contacting materials. Based on the experimental results, surface state models for the barrier height regulations of metal–dielectric and dielectric–dielectric pairs were proposed so as to deepen the understanding of essential mechanisms of CE.
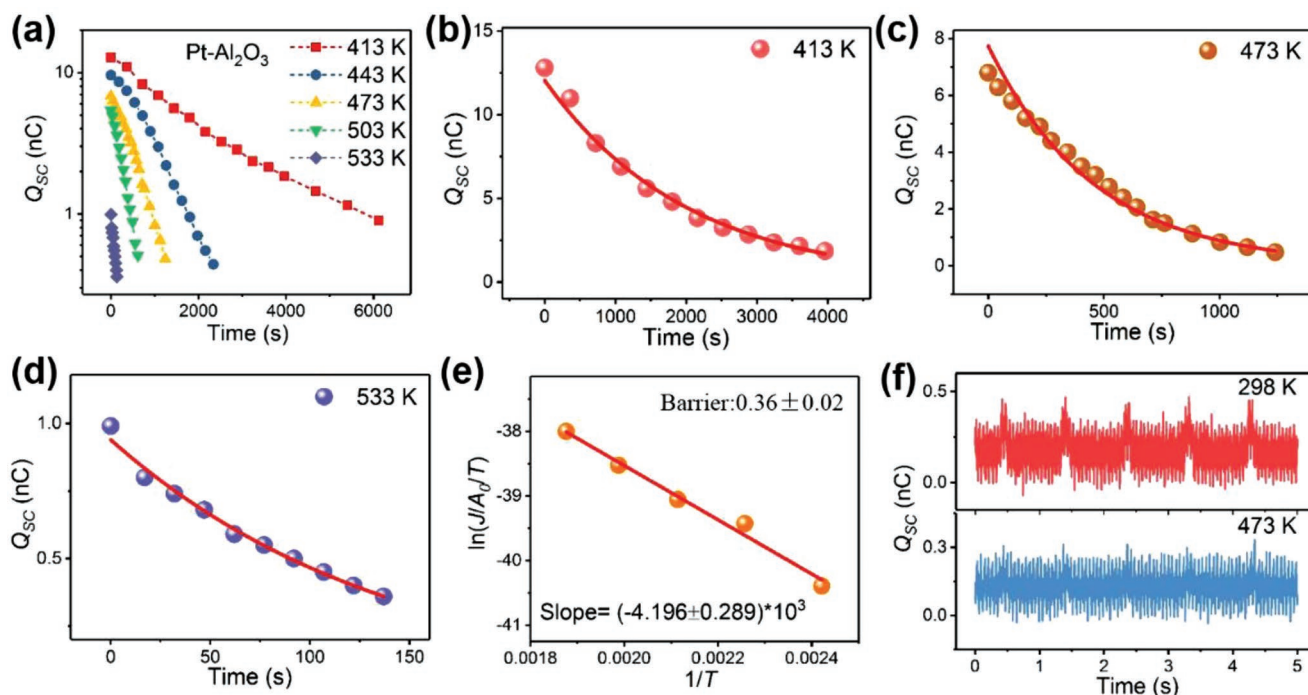
2. Results and Discussion

Figure 1a presents a high-temperature measurement platform for the TENGs. The heating cabinet provides desired temperatures with an accuracy of ±5 K. The section within the red-dashed frame in Figure 1a is the representative Pt-Al$_2$O$_3$ TENG with its enlarged image in Figure 1b and optical photograph in Figure 1c. Al$_2$O$_3$ and Pt coatings on Ti foil are the

electrification materials. Aside from Pt, Au, Ti, and Al are also utilized in the experiment and combined with Al$_2$O$_3$ to form an Au-Al$_2$O$_3$ TENG, Ti-Al$_2$O$_3$ TENG, and Al-Al$_2$O$_3$ TENG. Figure 1d shows the optical photographs of these metal materials. Figure 1e is the working principle of the Pt-Al$_2$O$_3$ TENG. When Pt and Al$_2$O$_3$ come into contact, opposite triboelectric charges are generated on the two surfaces with the same density: negative charges on Pt and positive charges on Al$_2$O$_3$. Upon releasing contact, the two oppositely charged surfaces start to become separate from each other, inducing a potential difference between the Pt and Au electrodes. This potential difference drives electron flow from the Pt to Au electrode. When the separation distance between the two surfaces reaches a maximum, almost all of the negative charges on Pt will be neutralized, so that the negative charges on the Au electrode equal the transferred charges on Pt. Subsequently, when Pt and Al$_2$O$_3$ approach each other again, a reversed potential difference between the two electrodes is built up, which leads to the back flow of all the transferred electrons from the Au electrode to Pt.

In the experiment, Al$_2$O$_3$ surface was first rubbed against polyurethane foam to be negatively charged with around 15 nC. Then, the cabinet was heated up to the desired temperature to measure the variation of short-circuit transfer charge Q_{SC} of the Pt-Al$_2$O$_3$ TENG. **Figure 2**a and Figure S1 in the Supporting Information show the long-term decay of Q_{SC} at temperatures of 413, 443, 473, 503, and 533 K, demonstrating that the charge density decreased more rapidly at higher temperatures. It also reveals that the Q_{SC} variation is analogous to exponential decay at high temperatures. This result accords with our previous research findings on Ti-SiO$_2$ at high temperatures.[21] To further explore whether the Q_{SC} variation of the Pt-Al$_2$O$_3$ TENG is consistent with the electron thermionic emission model, the measured Q_{SC} values in Figure 2a are fitted according to the thermionic emission equation[23,24]
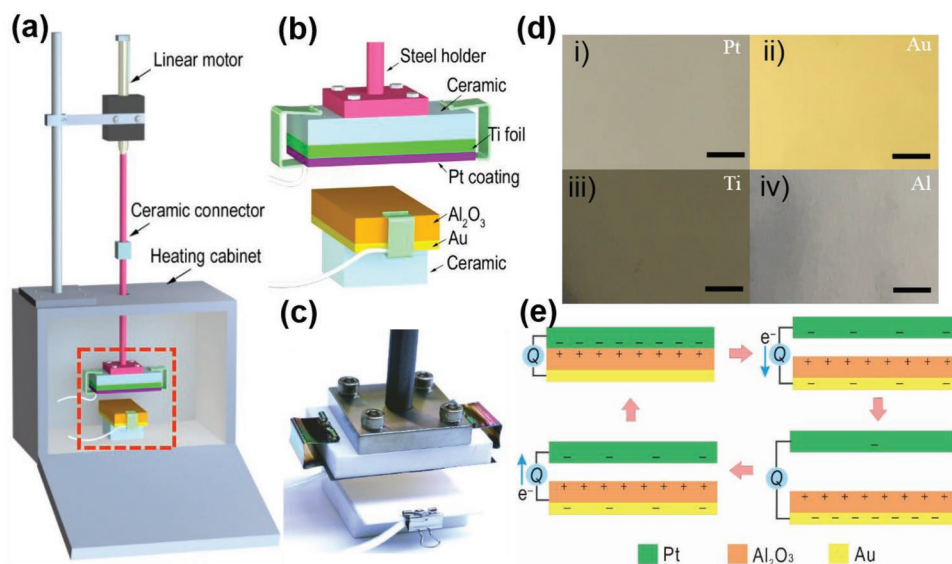
Figure 1. Setup of the high-temperature measurement platform for TENGs. a) Schematic illustration of the Pt-Al$_2$O$_3$ TENG in the platform. b,c) Enlarged view and optical photograph of the Pt-Al$_2$O$_3$ TENG within the red-dashed frame in (a). d) Optical photographs of Pt coating on Ti foil, Au coating on Ti foil, Ti foil, and Al foil. e) The working principle of the Pt-Al$_2$O$_3$ TENG.

ADVANCED
SCIENCE NEWS
www.advancedsciencenews.com

ADVANCED
FUNCTIONAL
MATERIALS
www.afm-journal.de

Figure 2. Experimental and simulated data of the Pt-Al$_2$O$_3$ TENG. a) Q_{SC} evolution with time at different temperatures. b–d) The measured (dots) and simulated (line) Q_{SC} as a function of the time at various temperatures of 413, 473, and 533 K. e) Plots of ln ($J/A_0/T$) against $1/T$. f) Q_{SC} generated by the TENG itself at 298 and 473 K.

$$J = \lambda A_0 T^2 e^{-\frac{W}{kT}}\left[e^{\frac{\Delta W}{kT}} - 1\right] \tag{1}$$

where J is the current density, λ is the material-specific correction factor, A_0 is Richardson constant of a free electron, T is the temperature, W is the height of the potential barrier, k is Boltzmann constant, and ΔW is the potential barrier height variation due to the surface electric field E. Here, we assume that $\Delta W = \lambda_1 Q_{SC}/\lambda$ (λ_1 is a constant), then

$$J = \frac{\lambda_1 A_0}{k} T e^{-\frac{qV}{kT}} Q_{SC} \tag{2}$$

where q is the electronic charge and V is the voltage. By assuming $J = \frac{1}{A}\frac{dQ_{SC}}{dt} = SQ_{SC}$, where A is the surface area and S is used to replace $\frac{\lambda_1 A_0}{k} T e^{-\frac{qV}{kT}}$, then

$$Q_{SC} = e^{-SAt} Q_{SC0} \tag{3}$$

where Q_{SC0} is the initial value of Q_{SC}. According to Equation (3), Q_{SC} follows an exponential decay during thermionic emission. Simulated charge decay curves at the typical temperatures of 413, 473, and 533 K are shown in Figure 2b–d, respectively. It shows that the simulated data are consistent with the measured data. In addition, provided that both sides of Equation (3) are transformed logarithmically at the same time, then

$$\ln\left[\frac{J}{A_0 T}\right] = -\frac{qV}{kT} + \ln\left[\frac{\lambda_1}{k} Q_{SC}\right] \tag{4}$$

According to Equation (4), the plots of ln ($J/A_0/T$) against $1/T$ are shown in Figure 2e. These plots illustrate that the measured data fit the thermionic emission equation very well. The height of the barrier W is calculated to be 0.36 ± 0.02 eV. Figure 2f is the Q_{SC} generated by the Pt-Al$_2$O$_3$ TENG itself at 298 and 473 K with the open-circuit voltage V_{OC} in Figure S2 in the Supporting Information. Since Pt is the reference to evaluate Al$_2$O$_3$, a positive sign of Q_{SC} indicates more negative charges on Pt than those on Al$_2$O$_3$. In other words, Pt is prone to obtaining electrons. Here, the measured Q_{SC} and V_{OC} of the Pt-PTFE TENG at 298 K further confirm this claim (Figure S3, Supporting Information). Because the electronegativity of PTFE is very large, the electrons flow from Pt to PTFE (i.e., Pt is more likely to lose electrons) when CE occurs. Through comparison of the Q_{SC} and V_{OC} of the above two types of TENGs, the electrons indeed flow from Al$_2$O$_3$ to Pt through the Pt-Al$_2$O$_3$ contact. Furthermore, the decreased Q_{SC} of the Pt-Al$_2$O$_3$ TENG at 473 K still indicates that the direction of electron transfer is the same as that at 298 K.

Figure 3a shows the Q_{SC} evolution of Au-Al$_2$O$_3$ TENG with time at different temperatures after introducing initial negative charges on the Al$_2$O$_3$ surface. Figure S4 in the Supporting Information exhibits the fitted curves at different temperatures according to the thermionic emission equation. Similar to what happens on the Pt-Al$_2$O$_3$ TENG, the fitted data coincide well with the experimental data. Figure 3b is the obtained plots of ln ($J/A_0/T$) against $1/T$ according to Equation (4), whose height of the barrier W is calculated to be 0.38 ± 0.01 eV. Figure 3c is the Q_{SC} generated by the Au-Al$_2$O$_3$ TENG itself at 298 and 473 K, which ensures that the direction of electron transfer at the Au-Al$_2$O$_3$ contact is from Al$_2$O$_3$ to Au, similar
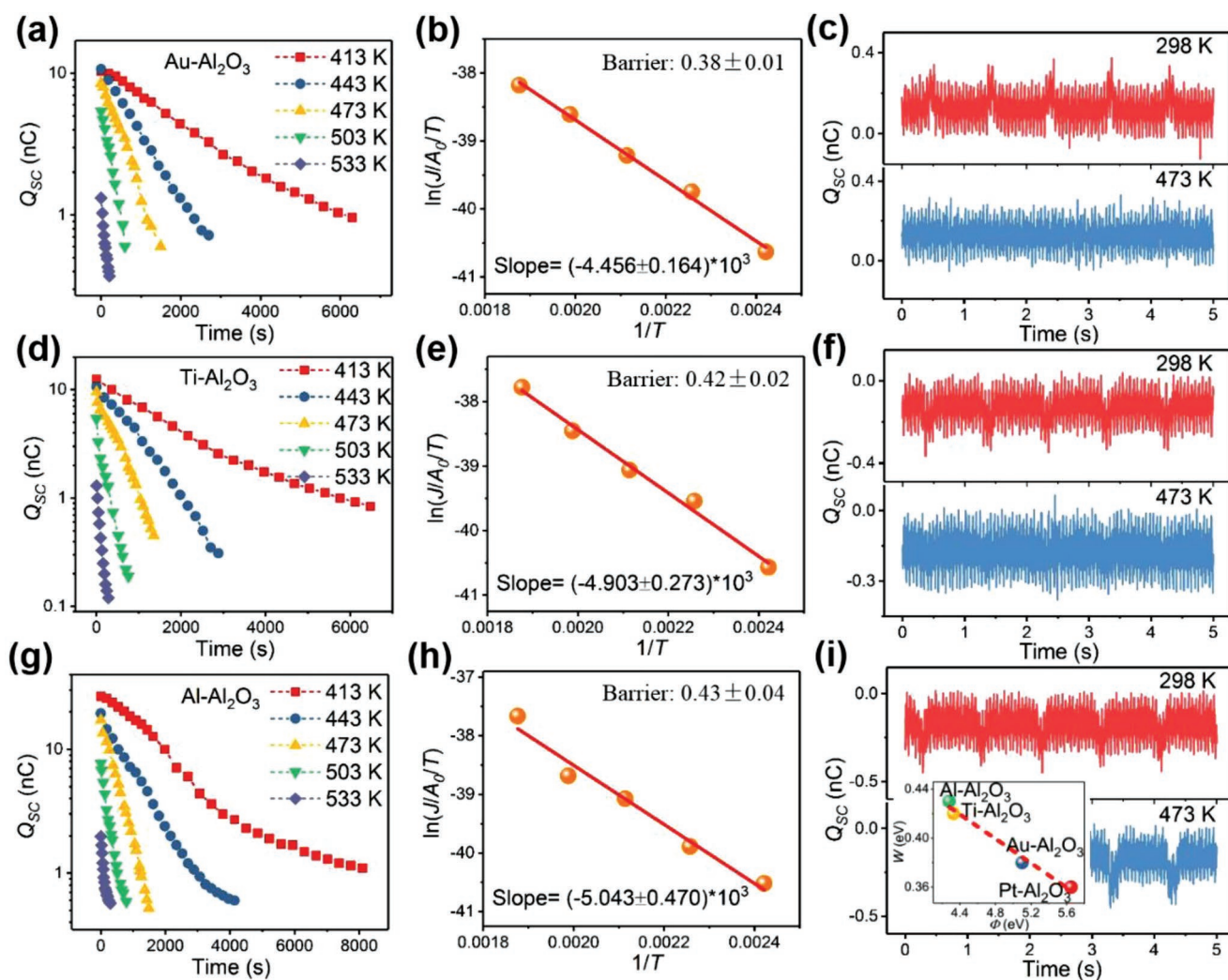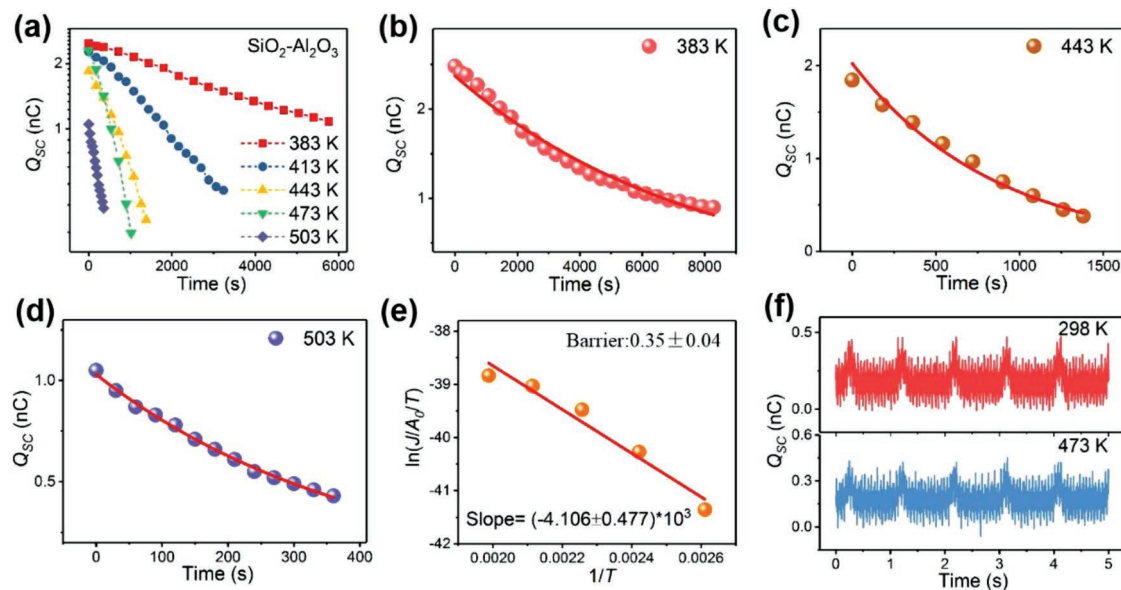
Figure 3. Performance of the $Au-Al_2O_3$ TENG, $Ti-Al_2O_3$ TENG, and $Al-Al_2O_3$ TENG. a–c) Q_{SC} evolution with time at different temperatures, plots of ln $(J/A_0/T)$ against $1/T$, and Q_{SC} generated by the $Au-Al_2O_3$ TENG. d–f) Q_{SC} evolution with time at different temperatures, plots of ln $(J/A_0/T)$ against $1/T$, and Q_{SC} generated by the $Ti-Al_2O_3$ TENG. g–i) Q_{SC} evolution with time at different temperatures, plots of ln $(J/A_0/T)$ against $1/T$, and Q_{SC} generated by the $Al-Al_2O_3$ TENG. Inset is the correlation between work functions of different metals and calculated barrier height of Al_2O_3.

to what happens on $Pt-Al_2O_3$ TENG. What is intriguing is that the Q_{SC} is too miniscule at 473 K to judge the direction of charge transfer. Figure 3d,g shows the Q_{SC} evolution of the $Ti-Al_2O_3$ TENG and $Al-Al_2O_3$ TENG at different temperatures after introducing initial negative charges, respectively. It should be noted that the heat resistance of Ti foil and Al foil is investigated before the experiment. After annealing at 573 K for 1 h, there was nearly no effect on the conductivity of both Ti foil and Al foil except some slight change of color on the surfaces. Therefore, the influence of the oxidation of Ti foil and Al foil on TENG performance is neglected in this experiment. Figures S5 and S6 in the Supporting Information exhibit the curves fitted by the thermionic emission equation. The fitted data are well consistent with the experimental data. The plots of ln $(J/A_0/T)$ against $1/T$ obtained from $Ti-Al_2O_3$ TENG are shown in Figure 3e, the barrier W of which is 0.42 ± 0.02 eV. Figure 3h shows that the barrier W of the $Al-Al_2O_3$ TENG is 0.43 ± 0.04 eV. It is noteworthy that when

the metals within both the $Ti-Al_2O_3$ TENG and $Al-Al_2O_3$ TENG contact with Al_2O_3, the directional flow of electrons is opposite to that within the $Pt-Al_2O_3$ TENG or $Au-Al_2O_3$ TENG, that is, it flows from Ti or Al to Al_2O_3 (Figure 3f,i). Previous studies indicated that the direction of charge transfer was relevant to the work function of metals when CE occurred at a metal–dielectric contact.[25] Here, the calculated barrier heights of materials also seem to be related to the work function of these contacted metals. The inset in Figure 3i displays the relationship between the work functions of three types of metals and barrier heights. The two present an inverse linear relation, that is, the barrier height decreases with the increase of the work function.

Besides the above metal–dielectric TENGs, SiO_2 deposited with an Au coating as a back electrode was utilized to form a $SiO_2-Al_2O_3$ TENG (i.e., dielectric–dielectric TENG). Similarly, initial charges were introduced to the surface of Al_2O_3 and then the long-term revolution of Q_{SC} was investigated at different

ADVANCED
SCIENCE NEWS
www.advancedsciencenews.com

ADVANCED
FUNCTIONAL
MATERIALS
www.afm-journal.de

Figure 4. Experimental and simulated data of the SiO_2-Al_2O_3 TENG. a) Q_{SC} evolution with time at different temperatures. b–d) The measured (dots) and simulated (line) Q_{SC} as a function of the time at various temperatures of 383, 443, and 503 K. e) Plots of ln $(J/A_0/T)$ against $1/T$. f) Q_{SC} generated by the TENG itself at 298 and 473 K.

temperatures. **Figure 4**a shows that the Q_{SC} resembles those on previously mentioned metal-Al_2O_3 TENGs: the speed of discharge accelerates with increase in temperature. Through fitting the electron thermionic emission equation, the fitted data at the temperatures of 383, 443, and 503 K in Figure 4b–d coincide well with the experiment data. This indicates the exponential decay of charges not only in metal–dielectric TENGs but also in dielectric–dielectric TENGs. Figure 4e shows that the calculated barrier W is 0.35 ± 0.04 eV. Figure 4f is the Q_{SC} generated by the SiO_2-Al_2O_3TENG itself at room temperature and high temperatures, indicating that electrons flow from Al_2O_3 to SiO_2 at the SiO_2-Al_2O_3 contact.

Through comparison among the values of barrier heights on the Al_2O_3 surfaces in the aforementioned five TENGs, it is found that the values are connected with the charge direction generated by the TENGs themselves. In other words, if the polarity of charges generated by a TENG is consistent with that of the introduced charges, the obtained barrier height will be higher (Ti-Al_2O_3 TENG and Al-Al_2O_3 TENG). However, if the polarity of charges generated by a TENG itself is opposite to that of the introduced charges, the barrier height will be lower (Pt-Al_2O_3 TENG, Au-Al_2O_3 TENG, and SiO_2-Al_2O_3 TENG). Since previous experiments only introduced negative charges on the surface of Al_2O_3 (Figures 2–4), the comparison experiment was conducted via the introduction of both positive and negative charges for further verification. **Figure 5**a,b shows Q_{SC} and V_{OC} evolution with time of Ti-Al_2O_3 TENG at 298 K after introducing initial negative (with polyurethane friction) and positive (with polytetrafluoroethylene friction) charges. The Q_{SC} and V_{OC} change slowly and with nearly the same trend, perhaps due to slower discharge at room temperature. Therefore, the temperature was increased to 443 K. As shown in Figure 5c, the Q_{SC} decreases more slowly with time by introducing negative charges than by introducing positive charges. This is mainly

because the electrons flow from Ti to Al_2O_3 when the two are in contact, which inhibits the velocity of electron thermionic emission from the surface of Al_2O_3. In other words, the increase of barrier height of the Al_2O_3 surface to some extent prevents negative charges from being lost. Figure 5d shows the Q_{SC} evolution of the SiO_2-Al_2O_3 TENG with time at 473 K after introducing initial positive or negative charges to the surface of Al_2O_3. The variation trend is opposite to that of the Ti-Al_2O_3 TENG: the decrease of positive charges is slower with time than that of negative charges. It is attributed to the fact that the directional flow of electrons generated by the SiO_2-Al_2O_3 TENG is from Al_2O_3 to SiO_2. Speeding up the rate of electron thermionic emission on the surface of Al_2O_3, that is, decreasing the barrier height to some extent, increases the likelihood of negative charge loss.

Based on the above findings, it is further confirmed that CE originates from electron transfer and the barrier height of a material's surface is a crucial factor for CE. It is important to note that the barrier heights of materials correlate with their contacting materials. Changing the contacting materials, whether to metals or dielectrics, is likely to alter the barrier height of the two materials in contact, and is termed "regulation." This regulation can be attributed to the work function or contact potential difference of the two contacted materials, which has an influence on the tendency or direction of electron transfer, which will be explained in detail via surface state models. **Figure 6**a–c displays the electron transfer yielded at the contact between a dielectric (with initial negative charges) and a metal. Figure 6a shows that the neutral level of surface states E_n in the dielectric is as high as the Fermi level E_f of the metal. When the two contact, due to CE an electron will hop over a barrier W from the dielectric to the metal surface. As shown in Figure 6b, if the metal has a greater work function Φ, there will be a difference of ΔE between E_n and E_f. Once the
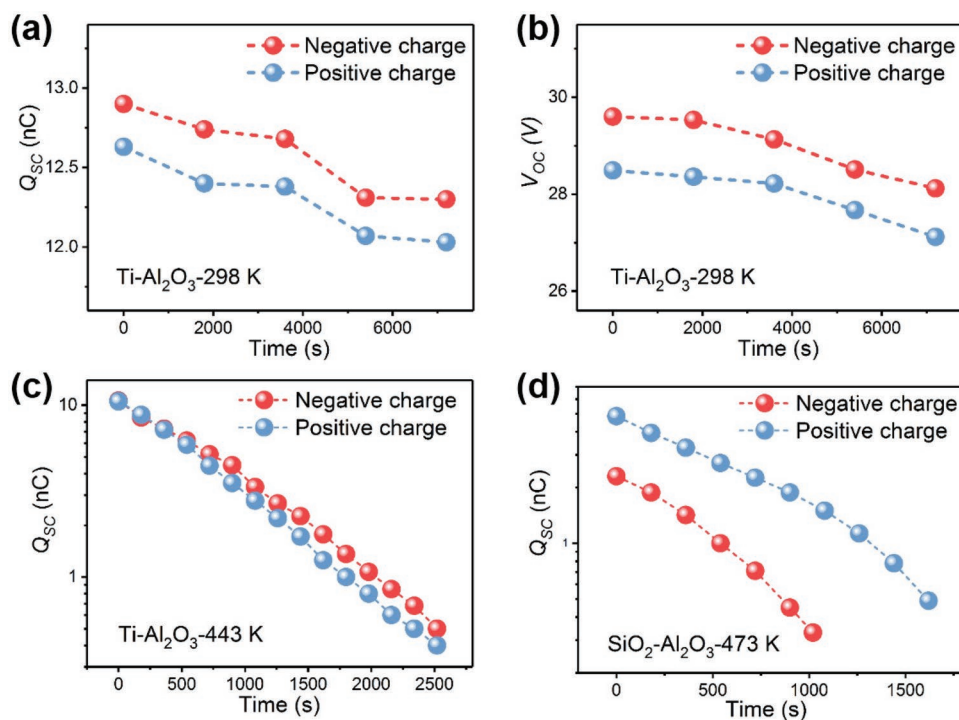
Figure 5. Comparison between the Q_{SC} evolution of the introduced initial negative charges and positive charges with time on TENGs. a,b) Q_{SC} and V_{OC} evolution with time of the Ti-Al$_2$O$_3$ TENG at 298 K. c) Q_{SC} evolution with time of the Ti-Al$_2$O$_3$ TENG at 443 K. d) Q_{SC} evolution with time of the SiO$_2$-Al$_2$O$_3$ TENG at 473 K.

metal and dielectric contact each other, an electron transfers to the metal surface via a hopping of a small barrier, namely, $W - \Delta E$. Suppose that the metal has comparatively small work function Φ (Figure 6c), its E_f will be ΔE of higher than E_n at the time. If the electron needs to transfer from the dielectric to the metal when the two contact, a greater barrier of $W + \Delta E$ would have to be overcome. The regulation of W at the dielectric–metal contact is also suitable for dielectric–dielectric CE. Figure 6d shows that when the E_n of dielectric A (with initial negative charges) and dielectric B are at the same level, the barrier that electron transfer needs to cross is W when the two contact. Given that the E_n of dielectric B is ΔE of lower than that of dielectric A, the barrier that the electron transfers over from dielectric A to dielectric B will reduce to $W - \Delta E$ (Figure 6e). Yet, supposing that the E_n of dielectric B is ΔE of higher than that of dielectric A, the barrier that the electron needs to transfer over from the latter to the former will be higher than $W + \Delta E$ (Figure 6f). These surface state models can help in better understanding of the regulation effect on the potential barrier height of materials and the electron transfer dominated mechanism in CE.

3. Conclusions

In summary, a variety of high-temperature-resistant TENGs such as metal–dielectric TENGs and dielectric–dielectric TENGs were prepared in this study. The results showed that the charge evolution at high temperatures of both metal–dielectric TENGs and dielectric–dielectric TENGs was in accord with

trends of electron thermionic emission model. Additionally, it was proposed for the first time that in the CE process, the potential barrier that electron transfer needs to cross was regulated by different contacting materials. This regulation lied in the fact that the work function or contact potential difference of the two materials had an influence on the tendency or direction of an electron hopping from one material to the other. Based on the above results, surface state models for CE of both metal–dielectric and dielectric–dielectric were formulated, respectively. These models further proved that electron transfer occurred in CE and deepened understanding of essential mechanisms of CE. Our study may provide a qualitative explanation for the charge amount generated by CE and offer guidance in selecting electrification materials for improving the efficiency of TENGs.

4. Experimental Section

Fabrication of TENGs: Ti foil (99.7%) with a thickness of 0.003 cm was purchased from Sigma-Aldrich Co. LLC. A 500 nm thick Pt or Au coating was deposited on Ti foil with a deposition rate of 0.2 nm s^{-1} by using a Denton Explorer E-beam Evaporator. After Pt deposition, Ti foil was annealed at 473 K for 2 h in air. Al$_2$O$_3$ (96%) with a thickness of 0.064 cm was purchased from MTI Corporation. The thermal conductivity was 24 W mK^{-1} at 293 K and the dielectric constant was 9.8 (293 K, 1 MHz). SiO$_2$ (99%) with a thickness of 0.318 cm was purchased from Technical Glass Products, Inc. The thermal conductivity was 1.4 W mK^{-1} at 293 K and the dielectric constant was 3.75 (293 K, 1 MHz). Polyurethane foam and polytetrafluoroethylene films were purchased from McMaster-Carr. The structure of Pt-Al$_2$O$_3$ TENG is shown in Figure 1a–c. The Pt and Al$_2$O$_3$ were used as the electrification materials. On the back of Al$_2$O$_3$,
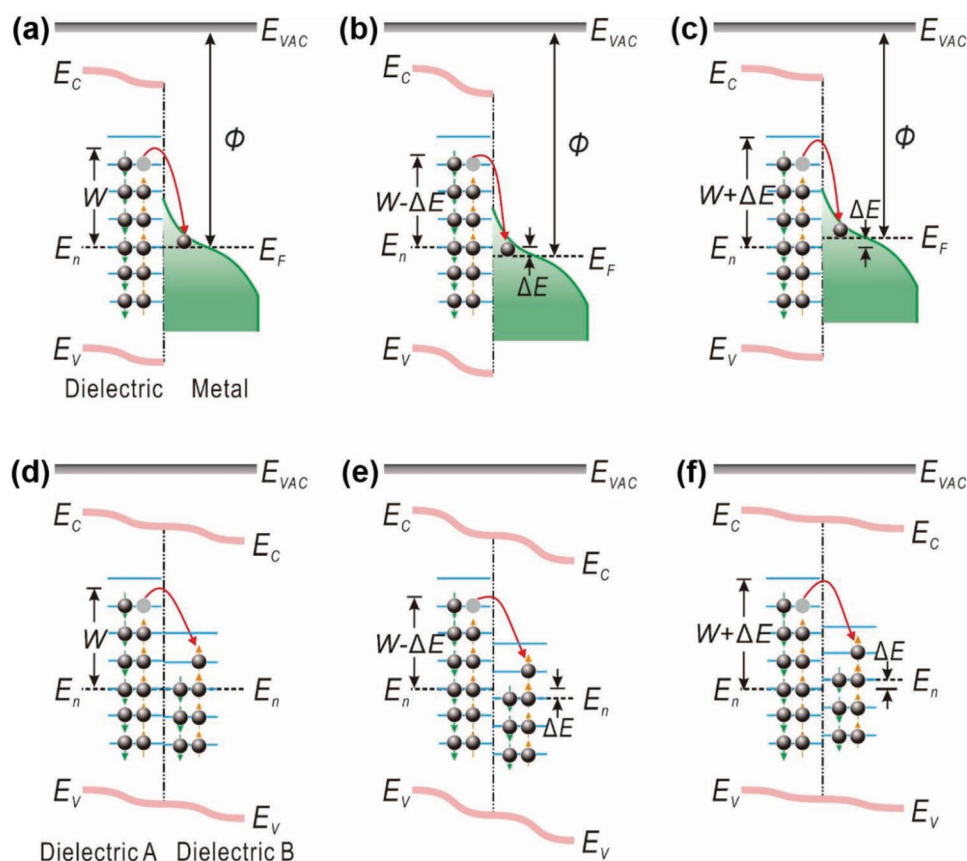
Figure 6. Surface state models for explaining the regulation of the potential barrier height of materials during CE, depending on the work function or contact potential difference of the contacted materials. Charge transfer between a dielectric (with initial negative charges) and a metal when E_n of the former is a) as high as, b) higher than, and c) lower than E_f of the latter. Charge transfer between dielectric A (with initial negative charges) and dielectric B when E_n of the former is d) as high as, e) higher than, and f) lower than that of the latter. E_{VAC}, vacuum level; E_C, conduction band; E_V, valence band; E_n, neutral level of surface states; W, potential barrier; Φ, work function; and E_F, Fermi level.

a 300 nm thick Au coating was deposited as an electrode. This Al_2O_3 was positioned on an insulating and high temperature resistant ceramic plate. In order to eliminate the interference of metal on the testing process, an insulating ceramic plate was specially added between the Ti foil over Al_2O_3 and the steel holder. For the Au-Al_2O_3 TENG, Ti-Al_2O_3 TENG, and Al-Al_2O_3 TENG, Ti foil with Pt coating was replaced by Ti foil with Au coating, Ti foil, and Al foil, respectively. The Al_2O_3 surfaces all had the same thickness as Au coating. The structures of the Au-Al_2O_3 TENG, Ti-Al_2O_3 TENG, Al-Al_2O_3 TENG, and SiO_2-Al_2O_3 TENG were the same as that of the Pt-Al_2O_3 TENG, except that the Ti foil with Pt coating was replaced by Ti foil with Au coating, Ti foil, Al foil, and SiO_2 with Au coating, respectively.

Measurement of TENGs: The TENGs were placed in a cabinet (Barnstead/Thermolyne 6000 furnace), which provided the desired temperature with an accuracy of ±5 K. The heating rate of the cabinet was about 7.5 K min^{-1}. As shown in Figure 1a, the top of the steel holder on the TENG extended out of the open hole on the heating cabinet and was connected with a linear motor. Between the steel holder and the linear motor, a connector was added for preventing the heat from damaging the linear motor. The environmental relative humidity was less than 30%. The loading force was about 2.1 N. The separation distance between the electrification materials of TENGs was 0.24 cm and the effective contact–separation areas of the TENGs were 18 cm^2. Relative humidity was tested by a Shaw Superdew 3 hygrometer. The short-circuit transfer charge Q_{SC} and open-circuit voltage V_{OC} of TENGs were measured by a Keithley 6514 electrometer.

Supporting Information

Supporting Information is available from the Wiley Online Library or from the author.

Conflict of Interest

The authors declare no conflict of interest.

[1] F. R. Fan, Z. Q. Tian, Z. L. Wang, *Nano Energy* **2012**, *1*, 328.

[2] Z. L. Wang, *Mater. Today* **2017**, *20*, 74.

[3] C. Wu, R. Liu, J. Wang, Y. Zi, L. Lin, Z. L. Wang, *Nano Energy* **2017**, *32*, 287.

[4] Z. Wu, H. Guo, W. Ding, Y.-C. Wang, L. Zhang, Z. L. Wang, *ACS Nano* **2019**, *13*, 377.

[5] W. Ding, A. C. Wang, C. Wu, H. Guo, Z. L. Wang, *Adv. Mater. Technol.* **2019**, *4*, 1800487.

[6] Y. Chen, Y. Zhang, Z. Wang, T. Zhan, Y.-C. Wang, H. Zou, H. Ren, G. Zhang, C. Zou, Z. L. Wang, *Adv. Mater.* **2018**, *30*, 1803580.

[7] H. Guo, X. Pu, J. Chen, Y. Meng, M.-H. Yeh, G. Liu, Q. Tang, B. Chen, D. Liu, S. Qi, C. Wu, C. Hu, J. Wang, Z. L. Wang, *Sci. Rob.* **2018**, *3*, eaat2516.

[8] P. Wang, R. Liu, W. Ding, P. Zhang, L. Pan, G. Dai, H. Zou, K. Dong, C. Xu, Z. L. Wang, *Adv. Funct. Mater.* **2018**, *28*, 1705808.

[9] S. L. Zhang, M. Xu, C. Zhanga, Y. Wang, H. Zou, X. He, Z. Wang, Z. L. Wang, *Nano Energy* **2018**, *48*, 421.

[10] Z. L. Wang, T. Jiang, L. Xu, *Nano Energy* **2017**, *39*, 9.

[11] Y. Zi, S. Niu, J. Wang, Z. Wen, W. Tang, Z. L. Wang, *Nat. Commun.* **2015**, *6*, 8376.

[12] C. X. Lu, C. B. Han, G. Q. Gu, J. Chen, Z. W. Yang, T. Jiang, C. He, Z. L. Wang, *Adv. Eng. Mater.* **2017**, *19*, 1700275.

[13] J. Lowell, *J. Phys. D: Appl. Phys.* **1975**, *8*, 53.

[14] W. R. Harper, *Proc. R. Soc. A* **1951**, *205*, 83.

[15] J. Lowell, *J. Phys. D: Appl. Phys.* **1977**, *10*, 65.

[16] C. Xu, B. Zhang, A. C. Wang, H. Zou, G. Liu, W. Ding, C. Wu, M. Ma, P. Feng, Z. Lin, Z. L. Wang, *ACS Nano* **2019**, *13*, 3545.

[17] D. J. Lacks, R. M. Sankaran, *J. Phys. D: Appl. Phys.* **2011**, *44*, 453001.

[18] H. A. Mizes, E. M. Conwell, D. P. Salamida, *Appl. Phys. Lett.* **1990**, *56*, 1597.

[19] L. S. McCarty, A. Winkleman, G. M. Whitesides, *J. Am. Chem. Soc.* **2007**, *129*, 4075.

[20] J. A. Wiles, M. Fialkowski, M. R. Radowski, G. M. Whitesides, B. A. Grzybowski, *J. Phys. Chem. B* **2004**, *108*, 20296.

[21] C. Xu, Y. Zi, A. C. Wang, H. Zou, Y. Dai, X. He, P. Wang, Y. Wang, Z. L. Wang, *Adv. Mater.* **2018**, *30*, 1706790.

[22] C. Xu, A. C. Wang, H. Zou, B. Zhang, C. Zhang, Y. Zi, L. Pan, P. Wang, P. Feng, Z. Lin, Z. L. Wang, *Adv. Mater.* **2018**, *30*, 1803968.

[23] C. Crowell, *Solid-State Electron.* **1965**, *8*, 395.

[24] J. Racko, A. Grmanová, J. Breza, *Solid-State Electron.* **1996**, *39*, 391.

[25] J. Lowell, A. C. Rose-Innes, *Adv. Phys.* **1980**, *29*, 947.